PAPER

Check for updates

Lateral flow immunochromatographic assay on a single piece of paper†

Xue Jiang [ID] [a] and Peter B. Lillehoj [ID] *[a,b]

Lateral flow immunochromatographic assays (LFIAs) are analytical devices used to detect the presence of one or more target analytes in a liquid sample. While LFIAs are one of the simplest and inexpensive types of immunoassays, they consist of multiple components (sample pad, conjugate pad, membrane, absorbent pad, backing card) and materials, requiring time-consuming device assembly. Here, we report a unique lateral flow immunochromatographic assay constructed from a single piece of cellulose paper, which is fabricated *via* laser cutting. Compared with conventional lateral flow immunochromatographic devices, this single-layer immunoassay enables simpler and faster fabrication, while minimizing material consumption and overall device costs. For proof-of-concept, this device was used to detect *Plasmodium falciparum* histidine-rich protein 2 (*Pf*HRP2), a biomarker for malaria infection, which could be detected at concentrations as low as 4 ng mL^{-1} by the naked eye with no cross reactivity with other common *Plasmodium* protein biomarkers. While offering similar speed and ease-of-use as conventional LFIAs with a higher detection sensitivity than existing LFIAs for *Pf*HRP2 detection, this single-layer lateral flow immunoassay has the potential to improve malaria testing, as well as the detection of other important protein biomarkers for point-of-care testing.

Introduction

Lateral flow immunochromatographic assays (LFIAs) are one of the simplest and most widely used biosensors for analytical detection. Compared with other types of immunoassays (enzyme-linked immunosorbent assay (ELISA), western blot), LFIAs are portable, inexpensive, provide rapid results (<20 minutes), and do not require complicated sample processing or the use of equipment.[1] Furthermore, LFIAs are compatible with a wide variety of biological matrices, including saliva,[2] urine,[3] semen,[4] serum[5,6] and whole blood.[6,7] For these reasons, LFIAs are commonly used for point-of-care diagnostic applications, such as home pregnancy testing and disease detection/screening.[8] Many rapid diagnostic tests (RDTs) for infectious diseases, including malaria,[9] HIV,[10] tuberculosis[11] and influenza,[12] are also based on LFIA architecture. In addition to medical testing, LFIAs are also widely used in veterinary medicine,[13,14] environmental monitoring,[15] food safety testing[16] and biological agent detection.[17,18]

LFIAs are comprised of several components, including a sample pad, conjugate release pad, membrane, absorbent pad and backing card.[19] Typically, each of these components is

made from a different material; cellulose fiber for the sample and adsorbent pads, glass fiber for the conjugate pad, nitrocellulose for the membrane, and polyvinyl chloride for the backing card.[20] Immunochromatographic test strips are assembled by overlapping the sample, conjugate and absorbent pads with the membrane in a sequential fashion, and mounting the entire assembly onto the backing card.[21] Most LFIAs are also enclosed in plastic cassettes to protect the test strip and provide visual indicators on the device to facilitate the testing process. While conventional LFIA architecture provides an effective means for simplified sample processing and rapid analyte detection, the use of multiple materials for the different components, and their assembly increases the time and costs associated with device fabrication. To simplify the fabrication of lateral flow immunochromatographic devices, Abe *et al.* reported an inkjet printing method to pattern microfluidic channels and immobilize capture antibodies on filter paper.[22] While this assay can be fabricated on a single piece of paper substrate, the inkjet patterning process requires several chemical treatment steps, and the limited resolution of the printed features hinders the analytical performance.

In this work, we demonstrate a unique strategy for fabricating a lateral flow immunochromatographic assay on a single piece of cellulose paper *via* laser cutting. All of the components of a traditional LFIA, such as the sample, conjugate and absorbent pads and membrane, are integrated on a cellulose paper assay card. The test strip geometry, composition of

ᵃDepartment of Mechanical Engineering, Rice University, Houston, TX 77005, USA. E-mail: lillehoj@rice.edu

ᵇDepartment of Bioengineering, Rice University, Houston, TX 77030, USA

†Electronic supplementary information (ESI) available: More supplementary data. See DOI: 10.1039/d0an02073g

the blocking solution, optical density (OD) of gold nanoparticles (AuNPs) and amount of AuNP-antibody conjugates were optimized to minimize nonspecific binding of AuNPs conjugates for enhanced detection sensitivity. The functionality of this immunoassay was validated by using it to detect *Plasmodium falciparum* histidine-rich protein 2 (*Pf*HRP2), a biomarker for malaria infection, which could be detected at concentrations as low as 4 ng mL^{-1} by the naked eye with excellent specificity. Based on this approach, the time, labor and material costs associated with LFIA fabrication can be greatly reduced, minimizing overall device costs and making LFIA development more accessible to researchers in academia and industry.

Materials and methods

Materials

Monoclonal mouse anti-*Plasmodium falciparum* HRP2 IgG and monoclonal mouse anti-*Plasmodium falciparum* HRP2 IgM were purchased from ICL (Portland, OR). Polyclonal rabbit anti-mouse IgG H&L was purchased from Abcam (Cambridge, United Kingdom). Recombinant *Pf*HRP2, Pan-*Plasmodium* aldolase and *Plasmodium falciparum* lactate dehydrogenase (*Pf*LDH) were purchased from CTK Biotech (Poway, CA). De-identified plasma from healthy human volunteers was purchased from BioIVT (Westbury, NY). All experimental methods involving plasma samples were in accordance with relevant human subjects protection and biosafety guidelines and regulations. Phosphate buffer saline (PBS), sucrose, Tween-20 and bovine serum albumin (BSA) were purchased from Sigma-Aldrich (St Louis, MO). StabilBlock® immunoassay stabilizer was purchased from Surmodics (Eden Prairie, MN). 40 nm OD 10 colloid gold nanoparticle solution (9×10^{11} particles per mL) was purchased from Expedeon (San Diego, CA). Whatman™ 3MM Chr chromatography paper was purchased from GE Healthcare (Chicago, IL). Medical grade adhesive tape was purchased from Adhesives Research, Inc. (Glen Rock, PA). Deionized (DI) water was generated using a Smart2Pure water purification system (Barnstead, Van Nuys, CA). Candle-Lite® candle wax was purchased from a local vendor.

Preparation of AuNP-IgG conjugates

12 μg of mouse anti-*Pf*HRP2 IgG at a stock concentration 9.28 mg mL^{-1} was added to 200 μL of 40 nm OD 10 colloid gold nanoparticle solution, vortexed for 30 seconds, agitated at 300 rpm for 30 minutes using an orbital shaker and incubated at room temperature for 20 minutes. 8 mg of BSA powder was added to the AuNP-IgG conjugate solution, which was agitated at 300 rpm for 30 minutes using an orbital shaker and incubated at room temperature for 20 minutes. The mixture was centrifuged at 6500*g* for 15 minutes, the supernatant was removed, and the precipitate was resuspended in 200 μL of 20% sucrose diluted in StabilBlock® immunoassay stabilizer with 0.25% Tween-20 (the AuNP-IgG conjugate solution had a

final AuNP OD of OD 10). The AuNP-IgG conjugate solution was stored at 4 °C prior to use.

Device fabrication

The geometry of the assay card was designed using Autodesk AutoCAD software and transferred to 3MM Chr chromatography paper using a Universal Laser System CO$_2$ laser cutter. The sample and conjugate release regions were treated with a blocking solution to prevent nonspecific binding of AuNP-antibody conjugates. Briefly, 15 μL of blocking solution was dropcasted 15 mm above the lower edge of the assay card, followed by drying at 37 °C for 15 minutes. This process was repeated four times. We observed that even if the blocking solution was applied slightly higher or lower on the strip, this assay still exhibited good reproducibility as long as the blocking solution did not spread to the test and control line region. 5 μL of AuNP-IgG conjugate solution was dispensed on the blocking solution-treated conjugate release region and dried at 37 °C for 1 hour. Mouse anti-*Pf*HRP2 IgM at 4 mg mL^{-1} and rabbit anti-mouse H&L IgG at 1 mg mL^{-1} were used for the test and control lines, respectively. Lines were hand drawn on the test strip using a fine tip (size 10/0) paintbrush at a velocity of ~20 mm s^{-1} and subsequently dried at 37 °C for 1 hour. The wax barrier was applied to the assay card by dipping the bottom edge of the card in molten wax (heated to 85 °C) to a depth of 4 mm, quickly removing it and allowing the wax to solidify.

Assay optimization

Experiments to optimize the blocking solution were carried out using solutions containing 20% (w/v) sucrose, 0.25% (w/v) Tween-20 and varying concentrations (1%, 2%, 3% or 4% w/v) of BSA in PBS. Test strips treated with these blocking solutions were used for measurements of *Pf*HRP2 at 0 ng mL^{-1}, 32 ng mL^{-1} and 1024 ng mL^{-1} in PBS. Experiments to optimize the width of the test strip were carried out by testing samples containing 32 ng mL^{-1} of *Pf*HRP2 in PBS using assay cards with varying strip widths (2 mm, 3 mm, 4 mm and 5 mm) treated with the optimized blocking solution (20% (w/v) sucrose, 0.25% (w/v) Tween-20 and 2% (w/v) BSA in PBS). Optimization of the AuNP-IgG conjugate amount was carried out by depositing varying volumes (3 μL, 5 μL, 8 μL or 10 μL) of AuNP-IgG conjugate solution on test strips treated with the optimized blocking solution, and performing measurements of samples containing *Pf*HRP2 at 16 ng mL^{-1} and 1024 ng mL^{-1} in PBS. Experiments were also performed to optimize the OD of AuNPs by testing PBS samples containing *Pf*HRP2 at 0 ng mL^{-1}, 16 ng mL^{-1} and 1024 ng mL^{-1} using assay cards containing AuNP-IgG conjugates with AuNP ODs of OD 3, OD 5, OD 8 or OD 10. For all assay optimization measurements, 45 μL of sample was dispensed on the sample region of the assay card, followed by 60 μL of PBS. The buffer solution was dispensed after the sample flowed through the test strip. Images of the assay cards after measurements were obtained using a Cannon CanoScan 9000F scanner.

*Pf*HRP2 immunoassay sensitivity and selectivity measurements

The sensitivity of the immunochromatographic assay was evaluated by testing plasma samples with increasing concentrations of *Pf*HRP2 from 0 to 1024 ng mL^{-1}. Recombinant *Pf*HRP2 was serially diluted in plasma and used for measurements without further processing. We evaluated the specificity of this assay by performing measurements of plasma samples containing *Pf*HRP2, Pan-*Plasmodium* aldolase (Pan) or *P. falciparum* lactate dehydrogenase (*Pf*LDH). Non-spiked human plasma was also tested as a blank control. For each measurement, 45 µL of sample was dispensed on the sample region, followed by 60 µL of PBS after the sample flowed through the test strip. Images of the assay cards after measurements were obtained using a Cannon CanoScan 9000F scanner.

Data analysis

Mean gray values were obtained from scanned images of assay cards as described in Khan *et al.*[23] Briefly, average gray values were calculated from RGB (red-green-blue) images using ImageJ software, and RGB gray values were converted to CMY (cyan-magenta-yellow) gray values using the formula: CMY gray value = 255 − RGB gray value. Therefore, gray values reported in this article are CMY gray values and higher gray values represent a darker color, indicating a higher concentration of AuNP conjugates. The mean gray value of the background color of the test strips was measured using a cropped area of 5 mm by 2 mm above and below test line, and the mean gray value of the test line was measured using a cropped area of 5 mm by 1 mm within the line.

Results and discussion

Selection of the paper substrate

We considered several different types of paper, including nitrocellulose membrane (Whatman FF120HP), cellulose chromatography paper (Whatman Grade 1 Chr and Whatman Grade 3MM Chr) and Fusion 5 membrane, for the development of the single-layer immunochromatographic device. The parameters that were considered during the selection process were the protein binding capability, capillary flow rate, paper thickness and material cost. A side-by-side comparison of these parameters for the four substrate materials considered for this device is presented in Table S1 in ESI.† In regards to lateral flow functionality, two important aspects of the substrate are the protein binding capability and blocking performance.[24] Nitrocellulose membrane and cellulose chromatography paper both offer excellent protein binding capabilities, enabling straightforward antibody immobilization *via* contact or non-contact dispensing/printing. In contrast, untreated Fusion 5 membrane exhibits poor protein binding and requires chemical treatment (*e.g.* pH modification) or the use of carrier beads for antibody immobilization.[25] Due to the excellent protein binding capability of nitrocellulose membrane and cellulose paper, a blocking step is required to passivate the test strip to minimize non-specific binding, whereas Fusion 5 membrane does not require a blocking step. While passivation of nitrocellulose membrane or cellulose paper using a blocking solution is a well-established and straightforward process,[24] antibody immobilization on Fusion 5 membrane requires the antibodies to be treated in an acidic solution or labeled using polystyrene beads, which can decrease antibody–antigen binding[26,27] and complicate device fabrication. Compared with cellulose paper, nitrocellulose membrane is more fragile and can crack if improperly handled, resulting in poor blocking performance and/or nonuniform liquid transport through the strip.[28] Therefore, cellulose paper offers a number of advantages over Fusion 5 membrane and nitrocellulose membrane in regards to simpler device fabrication and enhanced robustness.

Another important parameter that was considered was the capillary flow rate. Based on the manufacturers' specifications, the capillary flow rate in Whatman 1 Chr and 3MM Chr papers is ~0.07 mm s^{-1}, whereas the flow rates in Whatman FF120HP nitrocellulose membrane and Fusion 5 membrane are ~4–6× and ~14× faster, respectively. Prior work by Rivas *et al.* showed that slower flow rates in gold nanoparticle-based lateral flow assays could lead to enhanced immunocomplex formation at the beginning of the strip and at the test and control lines, resulting in higher detection sensitivity.[29] Therefore, Whatman chromatography paper appears to be more suitable for high sensitivity detection compared with nitrocellulose membrane or Fusion 5 membrane due to its slower capillary flow rate. Material cost was also considered during the selection process. Whatman 3MM Chr and Whatman 1 Chr are the most cost effective materials, costing ~$16 per m^2, which is 11× and 7× less expensive than Whatman FF120HP nitrocellulose membrane and Fusion 5 membrane, respectively. Of the two cellulose papers, Whatman 3MM Chr is nearly twice as thick as Whatman 1 Chr, which enables more liquid to be absorbed for the same surface area, resulting in a smaller device. Therefore, Whatman 3MM Chr is preferred over Whatman 1 Chr for creating a more portable device with less material usage.

Design of the single-layer immunochromatographic assay

Unlike conventional lateral flow immunochromatographic assays that are comprised of multiple components fabricated from different materials (cellulose fiber, glass fiber, nitrocellulose membrane and polyvinyl chloride), this immunochromatographic assay is fabricated from a single piece of cellulose paper, which greatly simplifies device fabrication and minimizes overall costs. As shown in Fig. 1, the device consists of an assay card encapsulated between two pieces of self-adhesive plastic film to protect it from the environment and minimize hazards associated with device handling. The assay card (Fig. 1B) consists of a sample region, a conjugate release region, a test strip containing test and control lines and an absorbent region. The conjugate release region contains anti-*Pf*HRP2 IgG antibodies labeled with AuNPs, and the test strip
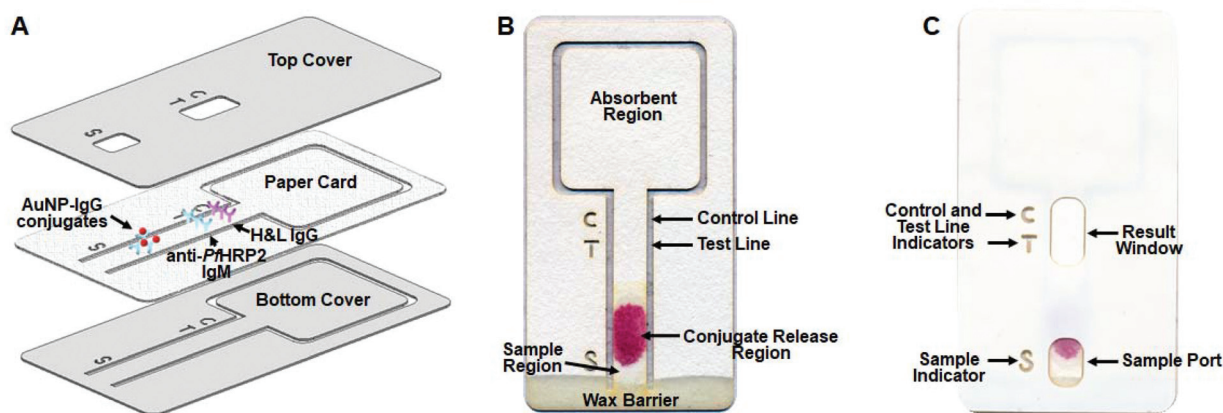
Fig. 1 (A) Exploded view of the single-layer lateral flow immunochromatographic assay. The assay card is encapsulated between two pieces of self-adhesive plastic film. Images of the immunochromatographic device without (B) and with (C) the plastic film.

contains immobilized anti-*Pf*HRP2 IgM antibodies and anti-mouse IgG H&L antibodies representing the test line and control line, respectively. The bottom of the test strip is connected to the outer structure of the assay card, allowing the sample, test and control line indicators to be incorporated directly on the paper card, while also facilitating alignment of the self-adhesive plastic film. The bottom of the card contains a hydrophobic wax barrier to prevent liquid backflow toward the outer structure of the card rather than toward the test and control lines, which could diminish the performance of the assay. The top plastic film contains cutouts for the sample dispensing port, test and control line indicators, and the result window (Fig. 1C).

Optimization of assay parameters

Several parameters, including the composition of the blocking solution, geometry of the test strip, OD of AuNPs and amount of AuNP-IgG conjugates applied to the conjugate release region, were optimized to enhance the sensitivity of this assay for *Pf*HRP2 detection. We first optimized the blocking solution by performing measurements of PBS samples containing varying concentrations of *Pf*HPR2 using assay cards that were treated with different blocking solutions. As shown in Fig. 2B–D, test strips treated with blocking solutions containing ≥2% (w/v) BSA generated test lines with similar color intensity at all *Pf*HRP2 concentrations. In contrast, the test lines of strips treated with the blocking solution containing 1% (w/v) BSA were noticeable lighter, particularly at 32 ng mL^{-1} (Fig. 2A). Mean gray values of the test strips confirm that those treated with the 2% (w/v) BSA blocking solution generated the lowest background signal, whereas strips treated with blocking solutions containing higher amounts of BSA generated higher background signals (Fig. 2E). Signal-to-background ratios (SBRs) calculated from mean gray values also reveal that test strips treated with the 2% (w/v) BSA blocking solution exhibit the highest SBRs at all antigen concentrations compared with strips treated with the other blocking solutions (Fig. 2F).
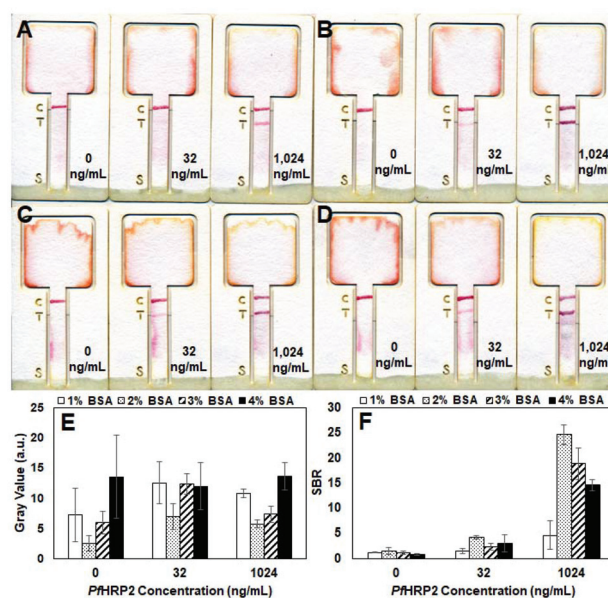

Fig. 2 Test results of samples containing 0 ng mL^{-1}, 32 ng mL^{-1} and 1024 ng mL^{-1} of *Pf*HRP2 in PBS using assay cards treated with blocking solution containing (A) 1% (w/v), (B) 2% (w/v), (C) 3% (w/v) or (D) 4% (w/v) of BSA. The plastic film is removed from the card for improved visualization of the test strip. (E) Mean gray values of the background color of test strips treated with different blocking solutions. (F) SBRs generated from mean gray values of the test line and background color of the test strips. Each bar represents the mean ± standard deviation (SD) of three measurements.

We investigated the influence of the test strip geometry on the detection sensitivity by performing measurements of PBS samples containing 32 ng mL^{-1} of *Pf*HRP2 using assay cards with varying strip widths. As shown in Fig. S1A,† the background color of the strips (which corresponds to the amount of AuNP-IgG conjugates remaining on the paper after dispensing the PBS flushing solution) is correlated with the width of the strip, where the narrower 2 mm- and 3 mm-wide strips exhibit dark background colors making the test line nearly

undetectable. In contrast, the background color of the 4 mm- and 5 mm-wide strips is significantly lighter, making the test line clearly observable. The narrower test strips exhibit a higher background color because the dried blocking and AuNP-IgG conjugate solutions act as a dissolvable barrier, which has been shown to increase the flow resistance and reduce the fluid flow speed in narrow paper strips.[30] Since the same amount of blocking and AuNP-IgG conjugate solutions are applied to all of the test strips, the narrower strips have a larger (*i.e.* longer) dissolvable barrier compared to wider strips. As a result, we observed that the liquid sample required a longer time to saturate the conjugate region on the narrower strips compared with the wider strips. Therefore, for the narrower strips, the sample tended to flow around the conjugate region due to the higher wettability of the untreated areas of the paper strip, causing a large amount of AuNP conjugates to remain on the strip thereby resulting a high background signal. In contrast, the liquid sample quickly saturated the conjugate region in the wider strips, enabling the AuNP-IgG conjugates to be readily transported to the absorbent region, resulting in a low background signal. Mean gray values of the test strips support the qualitative results shown in Fig. S1A,† where the 2 mm- and 3 mm-wide strips exhibit 3–5× higher background signals compared with the 4 mm- and 5 mm-wide strips (Fig. S1B†). The mean gray values of the test line were also obtained and used to calculate the SBR, which revealed that the 5 mm-wide strip generated the highest SBR (Fig. S1C†) of all the test strips, making it the optimal width.

Experiments were also carried out to optimize the amount of AuNP-IgG conjugates deposited on the assay card. Test strips with larger amounts (>5 µL) of AuNP-IgG conjugates produced more background color compared with those containing a smaller amount (<8 µL) of AuNP-IgG conjugates, particularity at lower (16 ng mL^{-1}) antigen concentrations (Fig. 3A). At higher (1024 ng mL^{-1}) antigen concentrations, the intensity of the test lines are dark and comparable for all test strips (Fig. 3B). Mean gray values show that the test strips containing 5 µL of AuNP-IgG conjugate solution generated the highest SBR for *Pf*HPR2 detection at 16 ng mL^{-1} (Fig. 3C) and at 1024 ng mL^{-1} (Fig. 3D). Based on these results, 5 µL was selected as the optimal AuNP-IgG conjugate solution volume, which provides the best analytical performance at both low and high concentrations of the target antigen. The last parameter that was optimized was the AuNP OD for AuNP-IgG conjugates. As shown in Fig. S2A–D,† assay cards containing AuNP-IgG conjugates with higher AuNP ODs generated darker test and control lines compared with those containing AuNP-IgG conjugates with lower AuNP ODs with no noticeable difference in the background color of the test strip. Mean gray values of the test line (Fig. S2E†) and SBRs calculated from mean gray values (Fig. S2F†) were also highest for assay cards containing AuNP-IgG conjugates with AuNP OD 10, which was selected as the optimal OD.

*Pf*HRP2 detection sensitivity and specificity

To evaluate the sensitivity (*i.e.* lower limit of detection, LOD) of this immunochromatographic assay, measurements were per-
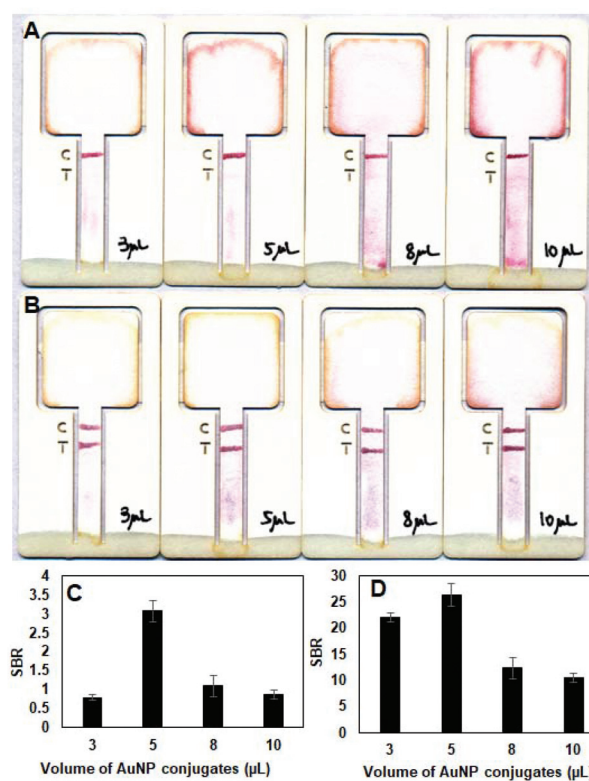

Fig. 3 Test results of samples containing 16 ng mL^{-1} (A) or 1024 ng mL^{-1} (B) of *Pf*HRP2 in PBS using assay cards deposited with 3 µL, 5 µL, 8 µL or 10 µL of AuNP-IgG conjugate solution. SBRs obtained from mean gray values of the test line and background color of the test strips at 16 ng mL^{-1} (C) and 1024 ng mL^{-1} (D) of *Pf*HRP2. Each bar represents the mean ± SD of three measurements.

formed using human plasma samples spiked with *Pf*HRP2 from 0 to 1024 ng mL^{-1}. As shown in Fig. 4A, the intensity of the test line is correlated with the *Pf*HRP2 concentration where samples containing lower amounts of antigen generated lighter test lines. All of the measurements generated a dark control line, validating the test results. Based on visual readout of the test results by the naked eye, this assay exhibits a LOD of 4 ng mL^{-1}, which is at least 2.5× lower than the LOD of previously reported lateral flow immunoassays for the detection of *Pf*HRP2 in plasma (10 ng mL^{-1}–31.2 ng mL^{-1}).[31,32] The improved detection sensitivity of our immunochromatographic device is likely due to the utilization of multiple optimized assay parameters, such as a wider strip width and higher AuNP OD for AuNP-IgG conjugates, compared with existing lateral flow immunoassays[22,31,33–35] which utilize smaller strip widths and/or lower AuNP ODs. Mean gray values of the test line (Fig. 4B) and SBRs calculated from mean gray values (Fig. 4C) also show a positive correlation between the test line intensity and the *Pf*HRP2 concentration, where the lowest detectable concentration is 4 ng mL^{-1}. Prior clinical studies have shown that *Pf*HRP2 levels in plasma of individuals with malaria infection range from 1 ng mL^{-1}–56 818 ng mL^{-1}, where the mean *Pf*HRP2 concentration in asymptomatic individuals is 19 ng
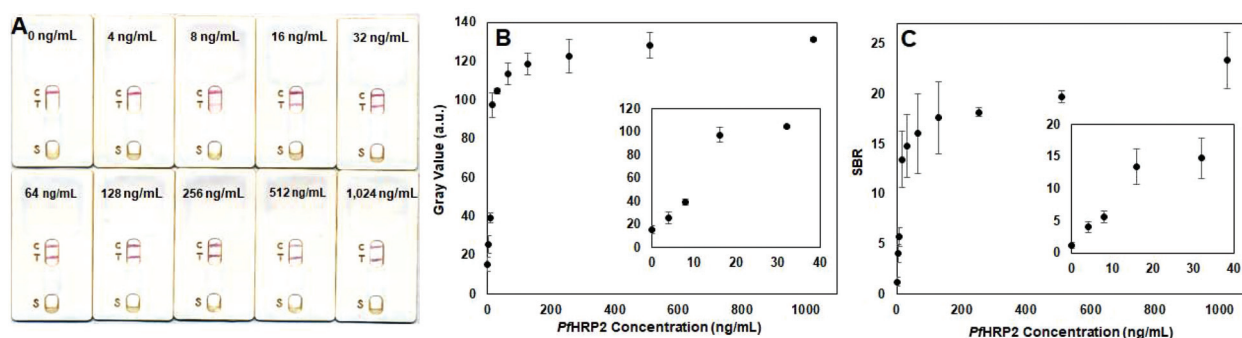
Fig. 4 (A) Test results of human plasma samples containing *Pf*HRP2 from 0 to 1024 ng mL^{-1}. (B) Mean gray values of the test line obtained from images in panel A. (C) SBRs generated from mean gray values of the test line and background color of the test strips in panel A. Each data point represents the mean $\pm$ SD of three measurements. Insets show magnified views of data points from 0 to 32 ng mL^{-1}.

mL^{-1}.[36] Therefore, the sensitivity of this assay makes it useful for detecting individuals with all severities of malaria disease, including asymptomatic infection, which cannot be achieved using commercial malaria RDTs due to their lower sensitivities (7–28 ng mL^{-1}).[37]

The specificity of the assay was assessed by evaluating its response to other common biomarkers of *P. falciparum* infection, including Pan-*Plasmodium* aldolase (Pan) and *P. falciparum* lactate dehydrogenase (*Pf*LDH). A non-spiked plasma sample was also tested and used as a blank control. As shown in Fig. 5A, only the *Pf*HRP2-containing sample generated dark test and control lines, denoting a "positive" test result. In contrast, only the control line was generated for samples containing the irrelevant proteins, similar with the non-spiked sample, denoting a "negative" result. These results demonstrate that this single-layer immunochromatographic

assay does not cross react with other common *Plasmodium* protein biomarkers in human samples, enabling highly specific detection of malaria infection.

Conclusions

We present a unique lateral flow immunochromatographic assay fabricated from a single piece of cellulose paper *via* laser cutting. This assay offers all of the advantages of lateral flow immunochromatographic technology while being simpler to assemble, less expensive, and offering higher detection sensitivity. Various assay parameters, including the test strip geometry, blocking solution composition, AuNP OD and amount of AuNP-antibody conjugates, were optimized to enhance the sensitivity of this single-layer immunochromatographic platform. Device characterization and testing revealed that this assay exhibits a lower detection limit of 4 ng mL^{-1} in human plasma, which is at least 1.75× more sensitive than commercial malaria RDTs, while exhibiting no cross-reactivity with other *P. falciparum* proteins. Furthermore, this analytical platform can be readily adapted to detect other biomarkers, making it a promising tool for point-of-care testing.

Author contribution statement

X.J and P.B.L. designed the experiments. X.J. performed the experiments. X.J. and P.B.L. analyzed the data and wrote the paper. All authors have given approval to the final version of the manuscript.

Fig. 5 (A) Test results of human plasma samples containing 1024 ng mL^{-1} of *Pf*HRP2, *Pf*LDH or pan-aldolase (Pan), and non-spiked human plasma. (B) Mean gray values of the test line obtained from images in panel A. Each bar represents the mean $\pm$ SD of three measurements.

Conflicts of interest

The authors declared no potential conflicts of interest with respect to the research, authorship, and/or publication of this article.
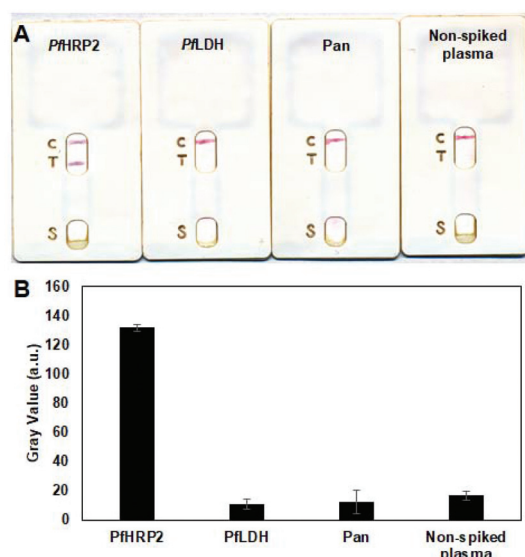
Acknowledgements

References

1 A. Chen and S. Yang, *Biosens. Bioelectron.*, 2015, **71**, 230–242.

2 J. B. Old, B. A. Schweers, P. W. Boonlayangoor and K. A. Reich, *J. Forensic Sci.*, 2009, **54**, 866–873.

3 V. S. Vaidya, G. M. Ford, S. S. Waikar, Y. Wang, M. B. Clement, V. Ramirez, W. E. Glaab, S. P. Troth, F. D. Sistare, W. C. Prozialeck, J. R. Edwards, N. A. Bobadilla, S. C. Mefferd and J. V. Bonventre, *Kidney Int.*, 2009, **76**, 108–114.

4 J. Old, B. A. Schweers, P. W. Boonlayangoor, B. Fischer, K. W. P. Miller and K. Reich, *J. Forensic Sci.*, 2012, **57**, 489–499.

5 H. L. Smits, T. H. Abdoel, J. Solera, E. Clavijo and R. Diaz, *Clin. Diagn. Lab. Immunol.*, 2003, **10**, 1141–1146.

6 E. I. Laderman, E. Whitworth, E. Dumaual, M. Jones, A. Hudak, W. Hogrefe, J. Carney and J. Groen, *Clin. Vaccine Immunol.*, 2008, **15**, 159–163.

7 B. A. Schweers, J. Old, P. W. Boonlayangoor and K. A. Reich, *Forensic Sci. Int.: Genet.*, 2008, **2**, 243–247.

8 R. Banerjee and A. Jaiswal, *Analyst*, 2018, **143**, 1970–1996.

9 E. Fu, T. Liang, P. Spicar-Mihalic, J. Houghtaling, S. Ramachandran and P. Yager, *Anal. Chem.*, 2012, **84**, 4574–4579.

10 B. A. Rohrman, V. Leautaud, E. Molyneux and R. R. Richards-Kortum, *PLoS One*, 2012, **7**, e45611.

11 M. Shah, C. Hanrahan, Z. Y. Wang, N. Dendukuri, S. D. Lawn, C. M. Denkinger and K. R. Steingart, *Cochrane Database Syst. Rev.*, 2016, **5**, CD011420.

12 N. M. Rodriguez, J. C. Linnes, A. Fan, C. K. Ellenson, N. R. Pollock and C. M. Klapperich, *Anal. Chem.*, 2015, **87**, 7872–7879.

13 Y. Al-Yousif, J. Anderson, C. Chard-Bergstrom and S. Kapil, *Clin. Diagn. Lab. Immunol.*, 2002, **9**, 723–724.

14 J. K. Oem, N. P. Ferris, K. N. Lee, Y. S. Joo, B. H. Hyun, J. H. Park, K. O. Jae, N. P. Ferris, K. N. Lee, Y. S. Joo, B. H. Hyun and J. H. Park, *Clin. Vaccine Immunol.*, 2009, **16**, 1660–1664.

15 Z. Mei, Y. Deng, H. Chu, F. Xue, Y. Zhong, J. Wu, H. Yang, Z. Wang, L. Zheng and W. Chen, *Microchim. Acta*, 2013, **180**, 279–285.

16 X. Wang, K. Li, D. Shi, N. Xiong, X. Jin, J. Yi and D. Bi, *J. Agric. Food Chem.*, 2007, **55**, 2072–2078.

17 F. Gessler, S. Pagel-Wieder, M. A. Avondet and H. Böhnel, *Diagn. Microbiol. Infect. Dis.*, 2007, **57**, 243–249.

18 S. Rong-Hwa, T. Shiao-Shek, C. Der-Jiang and H. Yao-Wen, *Food Chem.*, 2010, **118**, 462–466.

19 X. Huang, Z. P. Aguilar, H. Xu, W. Lai and Y. Xiong, *Biosens. Bioelectron.*, 2015, **75**, 166–180.

20 G. A. Posthuma-Trumpie and A. van Amerongen, in *Antibodies Applications and New Developments*, ed. G. A. Posthuma-Trumpie and A. van Amerongen, Bentham Science Publishers, 2012, pp. 175–183.

21 J. S. Ponti, in *Lateral Flow Immunoassay*, ed. R. Wong and H. Tse, Humana Press, Totowa, NJ, 2009, pp. 51–57.

22 K. Abe, K. Kotera, K. Suzuki and D. Citterio, *Anal. Bioanal. Chem.*, 2010, **398**, 885–893.

23 M. S. Khan, T. Pande and T. G. M. van de Ven, *Colloids Surf., B*, 2015, **132**, 264–270.

24 M. A. Mansfield, in *Lateral Flow Immunoassay*, ed. R. Wong and H. Tse, Humana Press, Totowa, NJ, 2009, pp. 95–113.

25 K. Jones, in *Lateral Flow Immunoassay*, ed. R. Wong and H. Tse, Humana Press, Totowa, NJ, 2009, pp. 115–129.

26 R. Reverberi and L. Reverberi, *Blood Transfus.*, 2007, **5**, 227–240.

27 W. Wang, S. Singh, D. L. Zeng, K. King and S. Nema, *J. Pharm. Sci.*, 2007, **96**, 1–26.

28 B. O'Farrell, in *Lateral Flow Immunoassay*, ed. R. Wong and H. Tse, Humana Press, Totowa, NJ, 2009, pp. 1–33.

29 L. Rivas, M. Medina-Sánchez, A. De La Escosura-Muñiz and A. Merkoçi, *Lab Chip*, 2014, **14**, 4406–4414.

30 B. Lutz, T. Liang, E. Fu, S. Ramachandran, P. Kauffman and P. Yager, *Lab Chip*, 2013, **13**, 2840–2847.

31 M. A. Nash, J. N. Waitumbi, A. S. Hoffman, P. Yager and P. S. Stayton, *ACS Nano*, 2012, **6**, 6776–6785.

32 J. Kim, X. E. Cao, J. L. Finkelstein, W. B. Cárdenas, D. Erickson and S. Mehta, *Malar. J.*, 2019, **18**, 1–10.

33 C. L. Mthembu, M. I. Sabela, M. Mlambo, L. M. Madikizela, S. Kanchi, H. Gumede and P. S. Mdluli, *Anal. Methods*, 2017, **9**, 5943–5951.

34 E. Fu, T. Liang, P. Spicar-Mihalic, J. Houghtaling, S. Ramachandran and P. Yager, *Anal. Chem.*, 2012, **84**, 4574–4579.

35 R. N. Deraney, C. R. Mace, J. P. Rolland and J. E. Schonhorn, *Anal. Chem.*, 2016, **88**, 6161–6165.

36 I. C. E. Hendriksen, L. J. White, J. Veenemans, G. Mtove, C. Woodrow, B. Amos, S. Saiwaew, S. Gesase, B. Nadjm, K. Silamut, S. Joseph, K. Chotivanich, N. P. J. Day, L. Von Seidlein, H. Verhoef, H. Reyburn, N. J. White and A. M. Dondorp, *J. Infect. Dis.*, 2013, **207**, 351–361.

37 L. Marquart, A. Butterworth, J. S. McCarthy and M. L. Gatton, *Malar. J.*, 2012, **11**, 74.